

TraHGR: Few-shot Learning for Hand Gesture Recognition via ElectroMyography

Soheil Zabihi, Elahe Rahimian, Amir Asif, and Arash Mohammadi

Abstract—Deep learning-based Hand Gesture Recognition (HGR) via surface Electromyogram (sEMG) signals has recently shown considerable potential for development of advanced myoelectric-controlled prosthesis. Although deep learning techniques can improve HGR accuracy compared to their classical counterparts, classifying hand movements based on sparse multichannel sEMG signals is still a challenging task. Furthermore, existing deep learning approaches, typically, include only one model as such can hardly maintain acceptable generalization performance in changing scenarios. In this paper, we aim to address this challenge by capitalizing on the recent advances of hybrid models and transformers. In other words, we propose a hybrid framework based on the transformer architecture, which is a relatively new and revolutionizing deep learning model. The proposed hybrid architecture, referred to as the Transformer for Hand Gesture Recognition (TraHGR), consists of two parallel paths followed by a linear layer that acts as a fusion center to integrate the advantage of each module and provide robustness over different scenarios. We evaluated the proposed architecture TraHGR based on the commonly used second Ninapro dataset, referred to as the DB2. The sEMG signals in the DB2 dataset are measured in the real-life conditions from 40 healthy users, each performing 49 gestures. We have conducted extensive set of experiments to test and validate the proposed TraHGR architecture, and have compared its achievable accuracy with more than five recently proposed HGR classification algorithms over the same dataset. We have also compared the results of the proposed TraHGR architecture with each individual path and demonstrated the distinguishing power of the proposed hybrid architecture. The recognition accuracies of the proposed TraHGR architecture are 86.18%, 88.91%, 81.44%, and 93.84%, which are 2.48%, 5.12%, 8.82%, and 4.30% higher than the state-of-the-art performance for DB2 (49 gestures), DB2-B (17 gestures), DB2-C (23 gestures), and DB2-D (9 gestures), respectively.

Index Terms—Electromyogram (EMG), Deep Neural Networks (DNNs), Machine Learning (ML), Transformers, Prosthetic, Classification, Hand Gesture.

I. INTRODUCTION

To improve the quality of life of people with upper limb amputation, recently, there has been a growing interest in development of learning-based myoelectric prostheses using multi-channel surface Electromyogram (sEMG) signals [1]–[3]. The information obtained from the sEMG signals, which are related to the neural activities of the underlying muscles, is used to decode the movements of the targeted limb. Generally speaking, sEMG signals can be collected via two different recording techniques, i.e., sparse multi-channel sEMG, and

S. Zabihi is with Electrical and Computer Engineering, Concordia University, Montreal, QC, Canada, H3G-2W1 (email: s_zab@encs.concordia.ca). E. Rahimian and A. Mohammadi are with Concordia Institute for Information System Engineering (CIISE), Concordia University, Montreal, QC, Canada, H3G-2W1 (emails: e_ahimia@encs.concordia.ca, arash.mohammadi@concordia.ca). A. Asif is with Electrical Engineering & Computer Science, York University, Toronto, Canada, M3J-1P3 (email: asif@eecs.yorku.ca).

High-Density sEMG (HD-sEMG). The former, typically, consists of a limited number of electrodes with sparse placement, which is the commonly used sEMG recording modality in wearable systems [4], [5]. On the other hand, a HD-sEMG device consists of a grid of electrodes that collect information about the temporal and spatial electrical activities of the underlying muscles enabling them to capture large amount of data [5]–[7]. This, however, results in increased complexity of the underlying system, which in turn challenges their ease of applicability in wearable systems and adds latency to the processing pipeline. Recent studies [8], therefore, focus on the use of sparse multi-channel sEMG devices given their ease of use and reduced complexity [9]. The use of sparse multi-channel sEMG datasets can, however, challenge the gesture recognition performance due to its sensitivity to the electrode location. In particular, while Deep Neural Networks (DNNs) achieve high performance in gesture recognition using HD-EMG devices, their efficacy is limited for sparse multi-channel sEMG devices in which a shallow dataset is collected with a lower sampling rate and limited number of electrodes. Inspired by the above discussion, as well as the significant gap between the performance of existing methods for HD-EMG and the sparse multi-channel sEMG approaches, the paper aims to present a new hybrid learning framework for achieving superior performance using sparse multi-channel signals.

Generally speaking, the developed methods for classifying hand movements can be classified into the following three main categories: (i) Traditional approaches based on Machine Learning (ML) architectures [10]–[14]; (ii) DNN-based techniques [5], [14]–[20], and; (iii) Hybrid methodologies [6] that combine multiple models. The common approach to perform Hand Gesture Recognition (HGR) in traditional methods (Case (i)) is to extract hand-crafted (engineered) features to train classical ML models such as Linear Discriminant Analysis (LDA), Support Vector Machine (SVM), and Random Forests (RF). In recent years, there has been a growth of interest in developing deep learning-based approaches (Case (ii)) for HGR, which show encouraging classification results [6], [21]. In particular, deep learning techniques provide an effective venue to automatically extract features from sEMG data and improve gesture recognition accuracy compared to their classical counterparts. However, many of the existing deep learning approaches involve only a single model, which can hardly maintain acceptable generalization performance in different scenarios, especially when configured for a specific scenario. The paper addresses this gap and focuses on the design of a transformer-based hybrid solution (Case (iii)) that has potentials for extracting temporal and spatial properties and improving HGR accuracy. In particular, transformer neural networks [22], which are a relatively new and revolutionizing

deep learning model, were first used for Natural Language Processing (NLP) tasks [23]. Recently, they have been used to improve the performance of several other applications such as Computer Vision (CV) [24] and speech recognition tasks [25]. Inspired by the recent advances of transformers in the various domains, in this paper, we aim to leverage the power of transformers to increase the HGR task performance.

Contributions: Motivated by the recent accomplishments of hybrid deep learning approaches, the paper proposes a hybrid DNN framework based on the transformer for the HGR task. Referred to as the Transformer for Hand Gesture Recognition (TraHGR), the proposed framework consists of two parallel paths (one Temporal transformer Network (TNet) and one Feature transformer Net (FNet)) followed by a linear layer, which integrates the output of each path to provide robustness across different scenarios. The TNet is used to extract temporal features while simultaneously the FNet is utilized to extract spatio-temporal features, which are then fused to augment the discriminating power of the model and improve the overall performance of HGR classification task. Performance of the proposed TraHGR framework is evaluated using the second Ninapro database [26]–[28] referred to DB2, which is a commonly used dataset that provides sparse multi-channel sEMG signals from various hand movements similar to those obtained in real-life conditions. Thus, Ninapro dataset enables development of innovative DNN-based recognition solutions for HGR task. We have conducted extensive set of experiments to test and validate the proposed TraHGR architecture, and compare its achievable accuracy with more than five recently proposed HGR classification algorithms based on the same datasets. Results show that the proposed TraHGR framework provides superior performance over all its counterparts. More specifically, the DB2 dataset has divided into 3 exercises with different hand gestures; i.e., DB2-B (17 gestures), DB2-C (23 gestures), and DB2-D (9 gestures). Our proposed architecture TraHGR outperforms all existing solutions over the DB2 dataset and its sub-exercises. In summary, the contributions of the paper are as follows:

- The paper for the first time, to the best of our knowledge, develops a hybrid Transformer based architecture for the task of HGR via sparse multi-channel sEMG.
- The paper demonstrates the superior performance of the proposed hybrid architecture TraHGR and its ability to extract more distinctive information for gesture recognition over the single models; i.e., TNet and FNet.
- The paper analyzes the effect of different window sizes 200ms, 150ms, and 100ms on overall performance and the model complexity.
- The paper classifies a high number (49) of gestures with a high accuracy. More specifically, compared with the proposed architectures in the recent state-of-the-art studies, TraHGR improves the recognition accuracies to 86.18% on DB2 (49 gestures), to 88.91% on the DB2-B (17 gestures), to 81.44% on DB2-C (23 gestures), and to 93.84% on the DB2-D (9 gestures).

The rest of the paper is organized as follows: In Section II, an

overview of related works is provided. Section III describes the database and pre-processing step. In Section IV, we present details of the proposed TraHGR architecture. The experiments and results are presented in Section V. Finally, the conclusion is presented in Section VI.

II. RELATED WORKS

The existing researches on prosthetic myoelectric control focus primarily on traditional ML approaches as a common strategy for HGR [29]. In such methods, handcrafted features, in time domain, frequency domain, or time-frequency domain [6], are first extracted by human experts, which are then fed to a ML classifier. Extraction and feature selection, however, can affect the overall performance [30], as such some researchers [5] have explored and integrated several classical feature sets that provide multi-view of sEMG signals to achieve higher gesture recognition accuracy. On the other hand, different classifiers such as SVM, LDA, RF, and Principal Components Analysis (PCA) are utilized in the literature [13], [14], [26], [30], [31] to increase the discriminating power of the model and improve gesture recognition performance.

Although the traditional ML-based approaches have shown strong potential for HGR task, more recently, there has been a great deal of interest in using deep-learning architectures to process multi-channel sEMG signals and increase the discrimination power of the model. In particular, it has been shown [14] that the automatic feature extraction used in deep learning architecture can lead to higher classification accuracy. More specifically, the authors in [14], for the first time, used the Convolutional Neural Network (CNN) architecture to classify hand gestures, which showed its potential to improve the overall performance compared to existing traditional approaches. This achievement was the starting point for considering CNN as a promising approach in the context of sEMG data classification [17], [20], [32]. For example, in Reference [7], the authors proposed and used the CNN architecture to extract spatial information from sEMG signals and perform HGR classification. In addition to CNN-based architectures, some researches [33], [34] used Recurrent Neural Networks (RNNs) to extract the temporal features from the sEMG signals. RNNs are used because sEMG signals are sequential in the nature, and recurrent-based networks such as Long Short Term Memory (LSTM) can extract the patterns in a sequence of sEMG data treating HGR as a sequence modeling task. In addition, it has been shown [35] that the proper design of CNN architectures can outperform RNNs in sequence modeling. In this respect, some researchers [8], [18], [19] used temporal convolutions for HGR and showed its potentials to extract temporal features.

Alternatively, hybrid architectures such as CNN-RNN have shown promising results in classifying hand movements [6], [16], as they benefit from advantages of different modules in extracting temporal and spatial features. Meanwhile, with the advent of the attention mechanism [22], transformers are being considered as a new ML technique for sequential data modeling [36], [37]. Capitalizing on the recent success of transformers in various fields such as machine translation [23],

[38], speech recognition [39] and computer vision [24], we aim to examine its applicability and potentials for sEMG-based gesture recognition. In other words, we recognized an urgent need to develop a transformer-based hybrid architecture to augment the recognition accuracy of HGR. In this paper, we introduce the TraHGR architecture, which increases the accuracy of sEMG decoding in the classification of human hand movements. In addition, we examine the complexity and performance of different types of TraHGR architectures.

III. MATERIAL AND METHODS

A. Database

The proposed TraHGR architecture is evaluated on the second Ninapro database [26]–[28], which is a publicly available dataset for sEMG-based human-machine interfacing. The second database Ninapro, which is referred to as the DB2, was collected from 40 users. Each user performs 49 movements in which each movement is repeated 6 times, each time lasting for 5 seconds, followed by 3 seconds of rest. The sEMG signals were gathered using Delsys Trigno Wireless EMG system with 12 wireless electrodes, sampled at 2 kHz. The DB2 dataset was presented in three exercises B, C, and D, which consist of different types of movements. In particular, Exercise B, C, and D consists of 17, 23, and 9 movements, respectively. For the rest of this paper, Exercise B, C, and D are referenced to DB2-B (17 gestures), DB2-C (23 gestures), and DB2-D (9 gestures), respectively. We followed the recommendations provided by previous studies [26]–[28] and consider the repetitions 1, 3, 4, and 6 of each movement as the training set, and the remaining repetitions, i.e., 2 and 5, as the test set.

B. Pre-processing Step

The EMG signals are pre-processed for classification purposes before being fed into the proposed architecture. The pre-processing phase consists of three steps, i.e., low-pass filtering, normalization, and segmentation. More specifically, we followed the procedure outlined in previous studies [7], [14], [21] and used the low-pass Butterworth filter. To enhance the performance of the proposed architecture, we applied the low-pass filter three times with different order of filters, namely 1, 3, and 5, and then concatenated all filtered signals together to form three-channel sEMG signals. Then, for the normalization step, we are inspired by the μ -law normalization technique introduced in [8], [17], which is defined as follows

$$F(x_t) = \text{sign}(x_t) \frac{\ln(1 + \mu|x_t|)}{\ln(1 + \mu)}, \quad (1)$$

where the input scaler is represented by x_t , and the new range of the signal is indicated by parameter μ . After normalization, the sEMG signals are segmented with a sliding window. More specifically, a common strategy used in previous studies is to segment sEMG signals with a window length that should be less than 300ms to meet an acceptable delay time [40] for practical applications. Therefore, in this study, the results are reported with three sliding windows of different lengths, i.e., 200ms, 150ms, and 100ms, each with a step size of 10ms. Each input from the sEMG signal segmentation phase is denoted by $\mathbf{X} \in \mathbb{R}^{S \times W \times C}$, where S shows the number of sensors in the

DB2 dataset, W shows the number of samples of electrical activities of muscles obtained at the rate of 2 kHz for a window of 200ms, 150ms, or 100ms, and C denotes the number of channels of the sEMG signals. This completes description of the pre-processing procedure. Next, the proposed TraHGR architecture is presented.

IV. THE TRAHGR FRAMEWORK

In this section, we explain details of the proposed TraHGR architecture for HGR. The TraHGR architectural design is based on transformers in which the attention mechanism is employed. The attention mechanism has been used in previous studies [6], [8], [18] in conjunction with CNNs and/or recurrent-based architectures for HGR task. However, in this paper, we show that transformer-based architectures that rely solely on attention mechanisms can perform better than previous studies in which CNN, RNN, and hybrid architectures (e.g., attention-based hybrid CNN-RNN) have been adopted. The overall proposed architecture is illustrated in Fig. 1, which is inspired by the Vision Transformer (ViT) [24], in which each input is divided into patches, and the network is supposed to perform label prediction based on the sequence of these patches. As shown in Fig. 1, the proposed TraHGR consists of a TNet path implemented in parallel with a FNet path followed by a linear layer, which acts as the fusion centre combining the extracted features from each of the two parallel paths in order to classify the hand gestures. In the following, we will further elaborate on the details of the proposed architecture.

A. Embedded Patches

In this sub-section, we focus on the input of the transformer encoder, which is a sequence of embedded patches. As illustrated in Fig. 1, the embedded patches are constructed from patch embeddings and position embeddings, which are described below.

1) *Patch Embeddings*: As mentioned earlier, we split each segment of sEMG signals \mathbf{X} into non-overlapping patches $\mathbf{X}_p = \{\mathbf{x}_p^i\}_{i=1}^N$. More specifically, each segment $\mathbf{X} \in \mathbb{R}^{S \times W \times C}$ is divided into N non-overlapping patches in which each patch is flattened. We represented the sequence of these flatten patches with $\mathbf{X}_p \in \mathbb{R}^{N \times (P_1 \cdot P_2 \cdot C)}$, where C denotes the number of channels, (P_1, P_2) shows the size of each patch, and $N = S \cdot W / P_1 \cdot P_2$ represents the length of this sequence, i.e., the number of patches. As shown in Fig. 1, we applied two types of patching:

- *Temporal Patching*: Here, the size of each patch is $(1, W)$; therefore, the number of patches is $N = S$. This type of patching is called Temporal Patching because each patch contains the information from only one of the sensors in the dataset for a sequence with length W . The TNet path is designed in such a way that they can take into account the temporal patches as the input.
- *Featural Patching*: We set the size of each patch to (S, S) , i.e., $P_1 = P_2 = S$, therefore, the number of patches is $N = W/S$. We refer to this type of patching as Featural because each patch contains the information of all S sensors for a sequence with length of S . Therefore,

both spatial and temporal information are included in a Featural patch. The Featural patches are provided as the input only to the FNet layer as shown in Fig. 1.

Finally, a linear mapping is introduced to create the embedding for each of these patches (Fig. 1). More specifically, a matrix $\mathbf{E} \in \mathbb{R}^{(P_1, P_2, C) \times D}$ is shared among different patches to linearly project each patch into the model dimension D (Eq. (2)). The output of this projection is known as the Patch Embeddings.

2) *Class Token*: Similar to the Bert framework [23], a trainable embedding is prepended to the sequence of patch embeddings ($\mathbf{Z}_0^0 = \mathbf{x}_{\text{class}}$) with the goal of capturing the meaning of the entire segmented input as a whole. More specifically, the class token's embedding after the last transformer encoder layer (\mathbf{Z}_L^0) is used for classification purposes (Eq. (10)).

3) *Position Embeddings*: As HGR based on sEMG signals is a time-series processing task, the order of data is an essential part for sequence modeling. Recurrent-based architectures such as LSTM inherently consider signal order, however, transformers do not process the input sequentially and combine the information of all the elements through attention mechanism. Therefore, there is a need to encode the order of each element in the sequence. This is where positional embedding comes in. In fact, position embedding allows the network to determine where a particular patch came from. There are several ways to retain position information at the transformer input, e.g., Sinusoidal positional embedding, 1-dimensional positional embedding, 2-dimensional positional, and Relative positional embeddings embedding [24], [39]. Following [24], we used the standard trainable 1-dimensional positional embeddings. As shown in Fig. 1, position embeddings indicated by $\mathbf{E}_{\text{pos}} \in \mathbb{R}^{(N+1) \times D}$ is added to the patch embeddings. The formulation which governs patch and position embeddings is as follows

$$\mathbf{Z}_0 = [\mathbf{x}_{\text{class}}; \mathbf{x}_p^1 \mathbf{E}; \mathbf{x}_p^2 \mathbf{E}; \dots; \mathbf{x}_p^N \mathbf{E}] + \mathbf{E}_{\text{pos}}. \quad (2)$$

The output of Eq. (2) is called Embedded Patches, which are fed as an the input to the transformer encoder.

B. Transformer Encoder

The transformer encoder takes the \mathbf{Z}_0 as an input. This block is inspired from the main transformer encoder introduced in [22], which treats all embedded patches as tokens. As illustrated in Fig. 1, the transformer encoder consists of L layers. Each layer contains two modules, namely the Multihead Self-Attention (MSA) and a Multi-Layer Perceptron (MLP) module, i.e.,

$$\mathbf{Z}'_l = \text{MSA}(\text{LayerNorm}(\mathbf{Z}_{l-1})) + \mathbf{Z}_{l-1}, \quad l = 1 \dots L \quad (3)$$

$$\mathbf{Z}_l = \text{MLP}(\text{LayerNorm}(\mathbf{Z}'_l)) + \mathbf{Z}'_l, \quad l = 1 \dots L \quad (4)$$

It is worth noting that a layer-normalization [41] is used before MSA and MLP modules, and the residual connections are applied to address degradation problem. The MLP module consists of two linear layers in which the first layer is followed by Gaussian Error Linear Unit (GELU) activation function. Moreover, the MSA module is defined based on the Self-Attention (SA) mechanism, which is discussed next.

1) *Self-Attention (SA)*: The SA mechanism [22] measures the pairwise similarity of each query and all the keys and obtains a weight for each value. Finally, the output is computed based on the weighted sum over of all values. In particular, if we define an input $\mathbf{Z} \in \mathbb{R}^{N \times D}$ consisting of N vectors, each of length D , the three matrices, i.e., Queries \mathbf{Q} , Keys \mathbf{K} , and Values \mathbf{V} , are calculated as follows

$$[\mathbf{Q}, \mathbf{K}, \mathbf{V}] = \mathbf{Z} \mathbf{W}_{QKV}, \quad (5)$$

where $\mathbf{W}_{QKV} \in \mathbb{R}^{D \times 3D_h}$ denotes the trainable weight matrix and D_h shows the length of each vector in \mathbf{Q} , \mathbf{K} , and \mathbf{V} . To measure the weights for \mathbf{V} , the dot-product of \mathbf{Q} and \mathbf{K} is calculated, then scaled with $\sqrt{D_h}$. These weights are converted to the probabilities $\mathbf{P} \in \mathbb{R}^{N \times N}$ using the softmax function as follows

$$\mathbf{P} = \text{softmax}\left(\frac{\mathbf{Q}\mathbf{K}^T}{\sqrt{D_h}}\right). \quad (6)$$

Finally, the output of SA mechanism is computed as follows

$$SA(\mathbf{Z}) = \mathbf{P}\mathbf{V}. \quad (7)$$

By using the attention mechanism, the model pinpoints a specific information in the input sequence.

2) *Multihead Self-Attention (MSA)*: Here, the SA mechanism is used for h times in parallel, allowing the architecture to pinpoint specific pieces of information in the input sequence for each head differently. In particular, each head has its own trainable weight matrix. The final matrix in the MSA mechanism is a projection of the concatenated outputs of the h heads, which is formulated as follows

$$MSA(\mathbf{Z}) = [SA_1(\mathbf{Z}); SA_2(\mathbf{Z}); \dots; SA_h(\mathbf{Z})] \mathbf{W}_{MSA}, \quad (8)$$

where $\mathbf{W}_{MSA} \in \mathbb{R}^{h \cdot D_h \times D}$. Here, D_h is set to D/h to keep the number of parameters constant when h changes.

C. TraHGR's Output

As shown in Fig. 1, the TraHGR consists of two paths, i.e., TNet and FNet. For each path, the aforementioned calculations (Eqs. (2)-(8)) are performed in parallel. Then, the predicted class labels of each path is calculated based on its corresponding \mathbf{Z}_L^0 as follows

$$y_{\text{path}} = \text{Linear}(\text{LayerNorm}(\mathbf{Z}_L^0)_{\text{path}}), \quad (9)$$

where $\text{path} \in \{\text{TNet}, \text{FNet}\}$. Finally, the output of the TraHGR is calculated based on the sum of \mathbf{Z}_L^0 in the TNet and FNet as follows

$$y = \text{Linear}(\text{LayerNorm}[(\mathbf{Z}_L^0)_{\text{TNet}} + (\mathbf{Z}_L^0)_{\text{FNet}}]). \quad (10)$$

It is worth mentioning that y_{TNet} , y_{FNet} , and y are used for TraHGR training. More details are provided in the sub-section V-A. This completes description of the proposed TraHGR architecture, next, its performance is evaluated through several experiments.

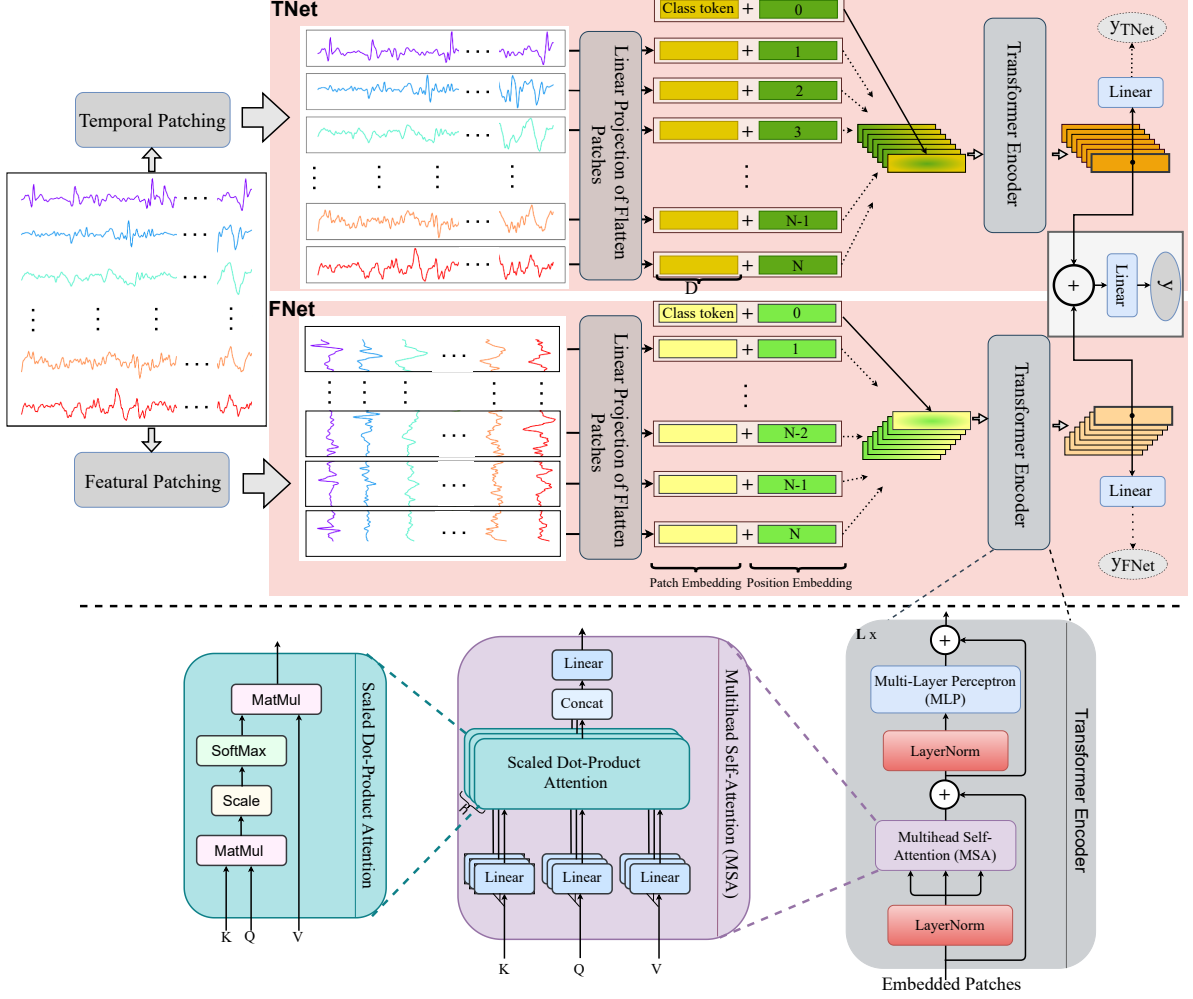


Fig. 1: **The proposed TraHGR architecture** consists of two parallel paths (one TNet and one FNet). Each segment of sEMG signals \mathbf{X} is divided into N non-overlapping patches. The TraHGR uses the TNet path to get the temporal patches while simultaneously the FNet is utilized to consider the featural patches. In both TNet and FNet, the patches are mapped linearly into the model dimension D . We refer to the output of this step as “Patch Embedding”. Then, a “class token” is prepended to the sequence of patch embeddings which is finally used for the classification purpose. The “Positional Embedding” is added to the “Patch Embedding” to retain the positional information. The output of this step is called “Embedded Patches” and is fed to the Transformer encoder consisting of L layers, each layer consisting of MSA and MLP modules. Finally, we add the output of the TNet and FNet class tokens to get the final representation, which then acts as the input to the linear layer.

TABLE I: Descriptions of TraHGR architecture variants, TNet, and FNet for DB2 (49 gestures). Number of parameters (Params) are reported for window sizes 200ms, 150ms, and 100ms.

Model	Layers (L)	Model dimension (D)	MLP size	Number of heads (h)	Params		
					200ms	150ms	100ms
TraHGR-Base	1	32	128	4	83,731	74,259	63,603
TraHGR-large	2	64	256	4	316,051	297,107	275,795
TraHGR-Huge	1	144	720	8	846,579	803,955	756,003
TNet	1	144	720	8	472,513	431,041	384,385
FNet	1	144	720	8	366,673	365,521	364,225

V. EXPERIMENTS AND RESULTS

In this section, we evaluate performance of the proposed TraHGR architecture through a series of experiments. In all experiments, the Adam optimizer [42] was used with learning rate of 0.0001 and the weight decay of 0.001. Moreover,

the batch size is set to 512. Table I shows different configurations of the hyperparameters in the TraHGR architecture resulting in different variants of the model denoted by TraHGR-Base, TraHGR-large, and TraHGR-Huge. These variants are then used for training and evaluation purposes with

TABLE II: The average of gesture recognition accuracy over all subjects using different window size (200ms, 150ms, and 100ms) for TraHGR architectures variants, TNet, and FNet for DB2 (49 gestures).

Model	Accuracy \pm STD		
	200ms	150ms	100ms
TraHGR-Base	78.60 \pm 6.03	77.54 \pm 5.99	76.17 \pm 6.09
TraHGR-large	83.58 \pm 5.48	82.58 \pm 5.60	81.30 \pm 5.87
TraHGR-Huge	86.18 \pm 4.99	85.43 \pm 5.24	84.13 \pm 5.21
TNet	83.39 \pm 5.44	82.81 \pm 5.60	81.43 \pm 5.88
FNet	80.72 \pm 5.82	80.05 \pm 6.03	79.38 \pm 6.15

window size $\in \{200ms, 150ms, 100ms\}$. Moreover, we evaluated the performance of a single deep model (TNet or FNet) when they are trained independently. In Table I, the number of parameters (Params) is calculated for DB2 (49 gestures) while this number will be less for DB2-B (17 gestures), DB2-C (23 gestures), and DB2-D (9 gestures).

A. Loss Function

The loss function \mathcal{L} of the TraHGR consists of the following three components

$$\mathcal{L} = \mathcal{L}_{TNet} + \mathcal{L}_{FNet} + \mathcal{L}_{TraHGR}, \quad (11)$$

where the first term \mathcal{L}_{TNet} is loss of the TNet path in the proposed TraHGR architecture. More specifically, cross-entropy loss is considered for measuring classification performance using the TNet's output y_{TNet} (Eq. (9)) and the target values. Similarly, the second term \mathcal{L}_{FNet} is the cross-entropy loss computed using the second path (FNet) of the TraHGR architecture where FNet's outputs y_{FNet} (Eq. (9)) are considered. Finally, the last term \mathcal{L}_{TraHGR} is calculated using the TraHGR's output y (Eq. (10)).

B. Evaluation of the Proposed TraHGR Architecture

This subsection provides evaluations on the prediction performance of the proposed hybrid transformer-based architecture. In this regard, first, we compare different variants of the TraHGR architecture and show the effect of different hyperparameters (e.g., number of layers, model dimension, MLP size, and number of heads) on the overall accuracy. Then, to demonstrate the performance of the hybrid transformer, we also compare the TraHGR architecture with single deep models, i.e., TNet and FNet.

Table II shows recognition accuracy, which is averaged over all subjects for the test set. From Table II, it can be observed that the proposed TraHGR-Huge architecture outperformed other TraHGR architecture variants (TraHGR-Base and TraHGR-large) when evaluated based on the DB2 (49 gestures) for the same window size. However, as shown in Table I, the number of parameters of the TraHGR-Huge is much higher than that of the TraHGR-Base and TraHGR-large models. This fact indicates that increasing the number of layers (l), model dimension (D), MLP size, and number of heads (h) have a positive effect on the model's

accuracy, however, this comes with the cost of increasing the complexity. In addition, as shown in Table I, each model has a larger number of trainable parameters for window size 200ms than its counterpart in the window size of 150ms or 100ms, resulting in a higher complexity. However, as shown in Table II, larger window size can further improve the results because the transformer in the proposed model has access to a longer sequence length.

We also trained and evaluated the proposed model for DB2-B (17 gestures), DB2-C (23 gestures), and DB2-D (9 gestures), independently. In Fig. 2, performance of the proposed architectures for DB2 (49 gestures) and its breakdown into three corresponding exercises, B, C, and D are shown. It can be observed that for both window sizes of 200ms and 150ms achieving a high accuracy for DB2-C (23 gestures) is a challenging task, while the model has achieved a high accuracy for DB2-B (17 gestures) and DB2-D (9 gestures). Moreover, as shown in Table II and Fig. 2, the proposed hybrid architecture TraHGR-Huge is more accurate than the single deep models (TNet and FNet). Therefore, the hybrid approach integrates advantages of two parallel paths through their integration such that the results can be aggregated to improve the predictive performance. It is worth mentioning that for hybrid models such as TraHGR-Base, TraHGR-large, and TraHGR-Huge, the classification accuracy is calculated using the output of Eq. (10), while for single deep models such as TNet and FNet this number is computed using the output of Eq. (9).

C. Statistical Analysis

For the window size 200ms, we performed statistical analysis on the effectiveness of the observations for DB2 (49 gestures). Therefore, following [8], [43], we considered each user as a separate dataset and conduct Wilcoxon signed-rank test [44]. According to the results shown in Fig. 3, the difference in accuracy between TraHGR-Huge and other proposed architectures such as TraHGR-Base, TraHGR-large, TNet, and FNet, for window sizes 200ms were considered statistically significant by the Wilcoxon signed-rank test. In Fig. 3, a p -value is annotated by the following markers: (i) $0.05 < p\text{-value} \leq 1$ is marked as not significant (ns); (ii) $0.01 < p\text{-value} \leq 0.05$ is depicted with *; (iii) $0.001 < p\text{-value} \leq 0.01$ is marked as **; (iv) $0.0001 < p\text{-value} \leq 0.001$ is shown with ***; and (v) $p\text{-value} \leq 0.0001$ is marked with ****. In Fig. 3, for each proposed model, the performance distribution over all users is illustrated. More specifically, each boxplot shows the Interquartile Range (IQR), which presents the performance of each model for all users into quartiles. The horizontal line in each boxplot illustrates the median performance.

D. Position-Wise Cosine Similarity

In Fig. 4(a) and (b), the position-wise cosine similarities between one position embedding and other embeddings are depicted for window sizes of 200ms and 150ms, respectively. In particular, close positions are brighter, that is, more similar, resulting in a matrix in which the main diagonal and its

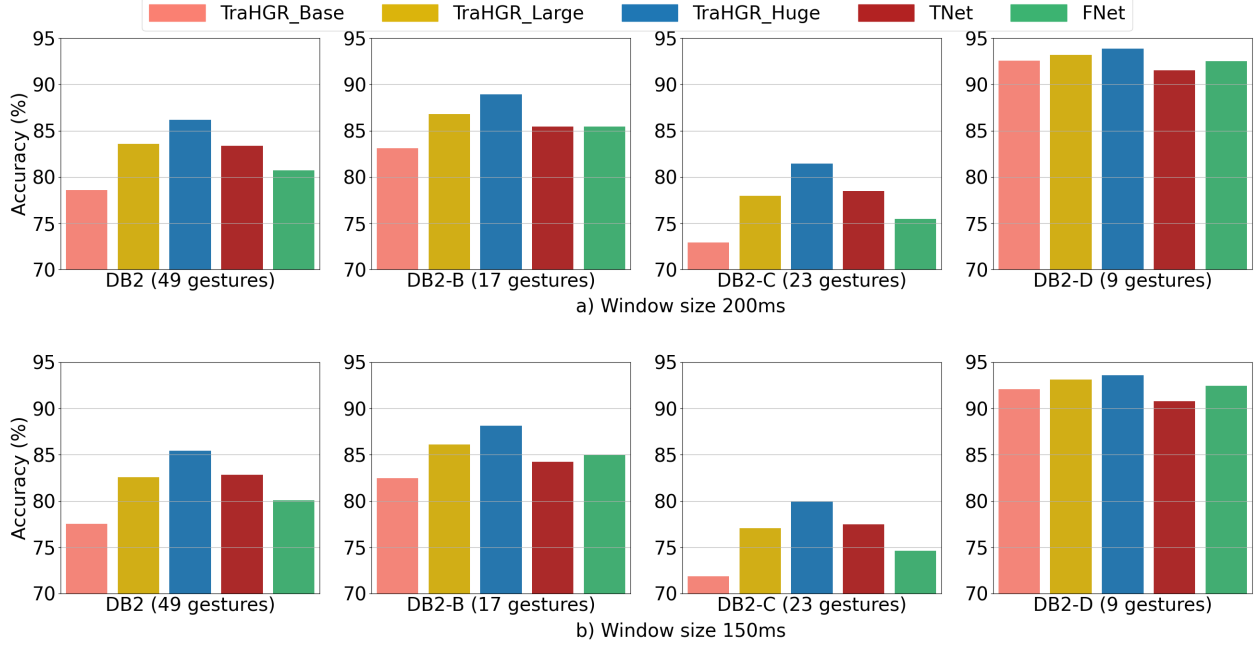


Fig. 2: Breakdown of DB2 (49 gestures) performance in DB2-B (17 gestures), DB2-C (23 gestures), and DB2-D (9 gestures) exercises.

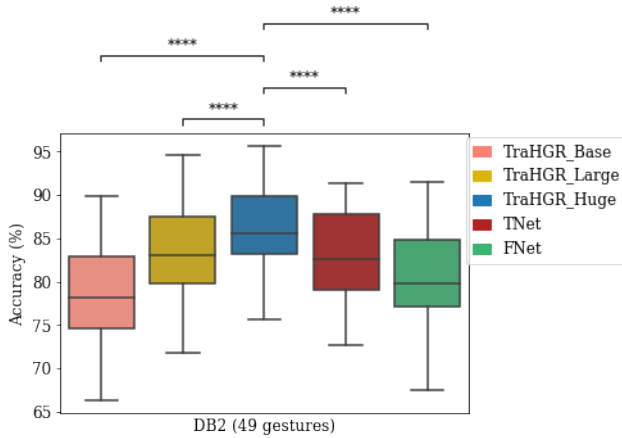


Fig. 3: The accuracy boxplots for all TraHGR architecture variants, TNet, and FNet for all 49 gestures in dataset Ninapro DB2. The IQR of each model is shown by a boxplot for all users. The Wilcoxon signed-rank test is used to compare the TraHGR-Huge with other architectures; i.e., TraHGR-Base, TraHGR-large, TNet, and FNet (ns: $0.05 < p \leq 1$, * : $0.01 < p \leq 0.05$, ** : $0.001 < p \leq 0.01$, *** : $0.0001 < p \leq 0.001$, **** : $p \leq 0.0001$).

neighbors have the brightest colors. As shown in Fig. 4, for both window sizes 200ms and 150ms, TraHGR-Huge captures the position meanings better than TraHGR-large, and TraHGR-large better than TraHGR-Base. As a result, we conclude that a more complex architecture can strengthen position embedding and include more location information for transformer encoders. Moreover, as shown in Fig. 4, for longer window sizes, the sequential nature of sEMG signals can be better encoded. For instance, as shown in Fig. 4(b), the position embeddings for TraHGR-Base architecture did not learn the meaning of positions completely. As a result, it can be concluded that the window size has a direct effect on obtaining position information for the transformer encoder.

E. Comparison with State-of-the-Art DNN Approaches

Table III provides a comparison between our proposed approach TraHGR-Huge and the available methodologies, which shows the superiority of the TraHGR architecture over the experimental results obtained from the state-of-the-art researches [5], [6], [14], [26], [31], [32]. This comparison was evaluated based on the same settings for the DB2 (49 gestures) dataset and its sub-exercises, i.e., DB2-B (17 gestures), DB2-C (23 gestures), and DB2-D (9 gestures). Descriptions of this database are provided in sub-section III-A. As stated previously, according to the recommendations in [40], the window size should be less than 300ms to meet the acceptable delay time for myoelectric control systems. Therefore, in this study, we segmented sEMG signals with three windows, i.e., 200ms, 150ms, and 100ms, to fulfill the mentioned limitation. As shown in Table III, our proposed approach TraHGR-Huge achieved higher accuracy than the existing methodologies when evaluated based on DB2 (49 gestures), DB2-B (17 gestures), DB2-C (23 gestures), DB2-D (9 gestures), and different time window sizes. More specifically, we compared the proposed architecture with both advanced DNNs and classical ML approaches.

For example, Reference [14] showed the average classification accuracy obtained using all the classical methods such as SVM, RF, K-Nearest Neighbors (K-NN), and LDA on the DB2 (49 gestures) dataset is 60.28%. They achieved the highest gesture recognition accuracy for RF which is 75.27%. Moreover, in Reference [31], they achieved the recognition accuracy 77.44% using SVM over all the movements. In addition, the recognition accuracy of 72.25% is reported in Reference [13] for the RF classifier. For DNN architectures, on the other hand, the best detection accuracy is reported in Reference [5] using CNN, which is 83.70%. As shown in

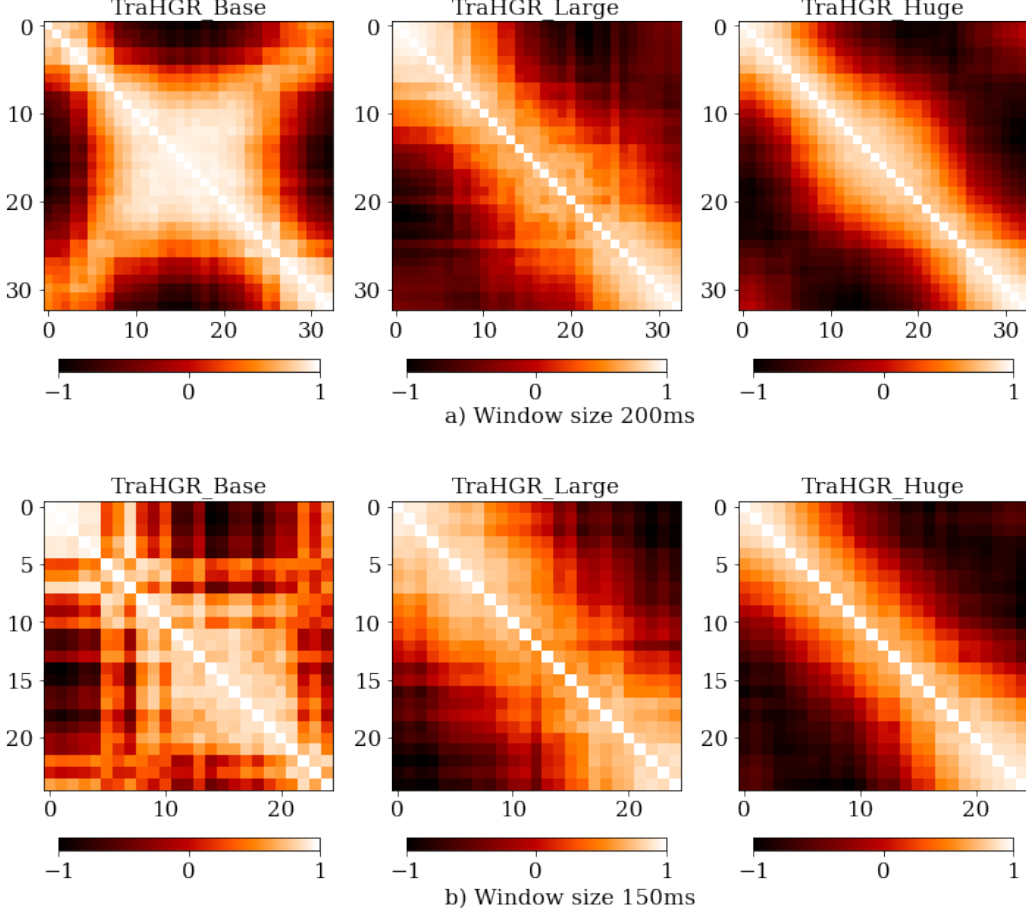


Fig. 4: Position embedding similarities for FNet path in TraHGR-Base, TraHGR-large, and TraHGR-Huge architectures: (a) window size is 200ms, and (b) window size is 150ms. Each row in each figure represents the cosine similarity between one embedding position and all the other embeddings. Brighter in the figures indicates more similarity.

Table III, for window size of 200ms, our proposed architecture achieved 86.18% classification accuracy which is 2.48% higher than the state-of-the-art DNN approach and 8.74% higher than state-of-the-art classical ML method. Moreover, it can be observed that for other window sizes, the classification accuracy of our proposed approach achieved better gesture recognition performances than its counterparts. For example, when the window size is set to 100ms, our proposed approach TraHGR-Huge was able to achieve gesture recognition accuracy of 84.13%, but using the proposed approach of [5], accuracy of 81.1% is achieved. It should be noted that the accuracy of 84.13% obtained by TraHGR-Huge with a window size of 100ms is still higher than the case where the window size in Reference [5] has doubled, i.e., 200ms. We also evaluated and compared our proposed method for DB2-B (17 gestures), DB2-C (23 gestures), and DB2-D (9 gestures) with the previous studies [31], [32], which demonstrates the superiority of our hybrid transformer-based framework.

F. Ablation Study

For the proposed hybrid architectures such as TraHGR-Huge, TraHGR-large, and TraHGR-Base, the classification accuracy is calculated using the prediction values y obtained from Eq. (10). To show that our proposed

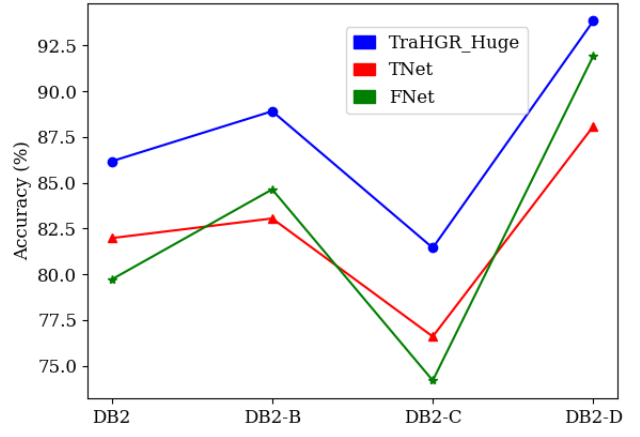


Fig. 5: The accuracy for TraHGR-Huge, TNet, and FNet when they are trained simultaneously for DB2 (49 gestures) and its sub-exercises, DB2-B (17 gestures), DB2-C (23 gestures), and DB2-D (9 gestures).

architecture based on a developed hybrid strategy has great potentials for improving gesture recognition accuracy, we also calculated the other two accuracies, i.e., $yTNet$ or $yFNet$, based on the Eq. (9). More specifically, we trained the hybrid architectures by computing the loss function in Eq. (11). However, output y is used to calculate the accuracy, reported

TABLE III: Comparison between our methodology (TraHGR-Huge) and previous works [5], [6], [14], [26], [31], [32].

Method	Database	Window size		
		200ms	150ms	100ms
CNN [5]	DB2 (49 gestures)	83.70	82.70	81.10
Attention-based Hybrid CNN-RNN [6]	DB2 (49 gestures)	82.20	-	-
CNN [32]	DB2 (49 gestures)	78.86	-	-
CNN [31]	DB2 (49 gestures)	78.71	-	-
CNN [14]	DB2 (49 gestures)	-	60.27	-
SVM [31]	DB2 (49 gestures)	77.44	-	-
RF [26]	DB2 (49 gestures)	75.27	-	-
RF [13]	DB2 (49 gestures)	72.25	-	-
TraHGR-Huge	DB2 (49 gestures)	86.18	85.43	84.13
CNN [31]	DB2-B (17 gestures)	82.22	-	-
CNN [32]	DB2-B (17 gestures)	83.79	-	-
SVM [31]	DB2-B (17 gestures)	81.07	-	-
TraHGR-Huge	DB2-B (17 gestures)	88.91	88.14	-
CNN [31]	DB2-C (23 gestures)	72.62	-	-
SVM [31]	DB2-C (23 gestures)	71.08	-	-
TraHGR-Huge	DB2-C (23 gestures)	81.44	79.99	-
CNN [31]	DB2-D (9 gestures)	89.54	-	-
SVM [31]	DB2-D (9 gestures)	88.56	-	-
TraHGR-Huge	DB2-D (9 gestures)	93.84	93.58	-

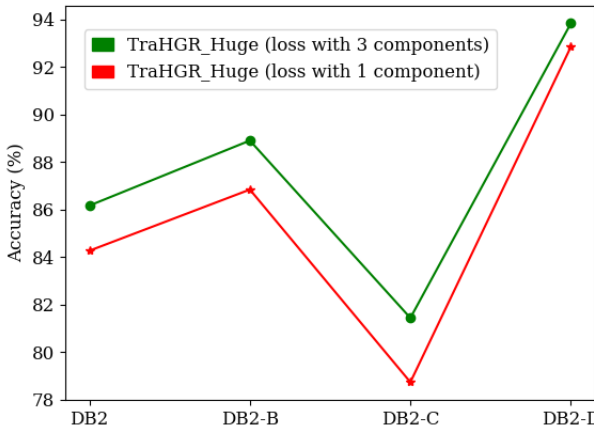


Fig. 6: Results of the ablation study on loss functions with TraHGR-Huge model which is trained by Eq. 11 (green) and Eq. 12 (red) evaluated on DB2 (49 gestures), DB2-B (17 gestures), DB2-C (23 gestures), and DB2-D (9 gestures).

in this paper. Here, in Fig. 5, it is shown that the accuracy obtained using the y is better than those calculated using the y_{TNet} or y_{FNet} for DB2 (49 gestures) and its sub-exercises. In particular, from Fig. 5, it can be observed that the hybrid architecture takes advantage of two parallel paths and improved the recognition accuracy.

1) *Evaluation of Different Loss Functions:* As described in sub-section V-A, our proposed hybrid architectures' param-

eters are learned by optimizing the loss function \mathcal{L} , which consists of three components. To demonstrate the advantage of training our proposed hybrid architecture with loss function \mathcal{L} defined in Eq. (11), we evaluated performance of TraHGR-Huge when the loss function \mathcal{L} has only one component as follows

$$\mathcal{L} = \mathcal{L}_{\text{TraHGR}}. \quad (12)$$

Fig. 6 shows the performance of TraHGR-Huge in DB2 (49 gestures) and its sub-exercises for two different loss functions. We can see that training TraHGR-Huge with a loss function with three components (Eq. (11)) improves the results compared to the case where loss function \mathcal{L} has only one component (Eq. (12)).

VI. CONCLUSION

In this paper, we proposed a hybrid architecture based on transformers for the task of hand gesture recognition. We have shown that the proposed hybrid architecture, referred to as the TraHGR framework, could augment the power of model discrimination in different scenarios for various exercises. Moreover, we investigated the ability of transformers for sEMG-based hand gesture recognition as they have revolutionized other fields such as NLP, CV, and speech recognition. In this regard, we compared TraHGR results with traditional ML approaches and DNN-based techniques and demonstrated

the outstanding performance of the proposed architecture. A potential direction for future research is to use the proposed transformer-based architecture to develop an adaptive learning method with focus on increasing the robustness of sEMG classifiers and improving inter-subject accuracy will be an interesting direction for future research. Another direction for future research is to use and extend the proposed transformer-based hybrid architecture to other machine learning fields.

REFERENCES

- [1] N. Jiang, S. Dosen, K.R. Muller, D. Farina, "Myoelectric Control of Artificial Limbs- Is There a Need to Change Focus?" *IEEE Signal Process. Mag.*, vol. 29, pp. 150-152, 2012.
- [2] D. Farina, R. Merletti, R.M. Enoka, "The Extraction of Neural Strategies from the Surface EMG," *J. Appl. Physiol.*, vol. 96, pp. 1486-95, 2004.
- [3] D. Farina, N. Jiang, H. Rehbaum, A. Holobar, B. Graimann, H. Dietl, and O. C. Aszmann, "The Extraction of Neural Information from the Surface EMG for the Control of Upper-limb Prostheses: Emerging Avenues and Challenges..," *IEEE Trans. Neural Syst. Rehabil. Eng.*, vol. 22, no.4, pp. 797-809, 2014.
- [4] M. Ergeneci *et al.*, "An embedded, eight channel, noise canceling, wireless, wearable sEMG data acquisition system with adaptive muscle contraction detection," *IEEE Trans. Biomed. Circuits Syst.*, vol. 12, no. 1, pp. 68-79, Feb. 2018.
- [5] W. Wei *et al.*, "Surface Electromyography-based Gesture Recognition by Multi-view Deep Learning," *IEEE Trans. Biomed. Eng.*, vol. 66, no. 10, pp. 2964-2973, 2019.
- [6] Y. Hu *et al.*, "A Novel Attention-based Hybrid CNN-RNN Architecture for sEMG-based Gesture Recognition," *Plos one* 13, no. 10, 2018.
- [7] W. Geng, *et al.*, "Gesture Recognition by Instantaneous Surface EMG Images," *Scientific Reports*, 6, p. 36571, 2016.
- [8] E. Rahimian, S. Zabihi, A. Asif, D. Farina, S.F. Atashzar, and A. Mohammadi, "FS-HGR: Few-shot Learning for Hand Gesture Recognition via ElectroMyography," *IEEE Trans. Neural Syst. Rehabil. Eng.*, 2021.
- [9] A. Stango, F. Negro, and D. Farina, "Spatial Correlation of High Density EMG Signals Provides Features Robust to Electrode Number and Shift in Pattern Recognition for Myocontrol," *IEEE Trans. Neural Syst. Rehabil. Eng.*, vol. 23, no. 2, pp.189-198. 2014.
- [10] D. Esposito *et al.*, "A Piezoresistive Array Armband with Reduced Number of Sensors for Hand Gesture Recognition," *Frontiers in Neurorobotics*, vol. 13, p. 114, 2020.
- [11] M. Tavakoli, C. Benussi, P.A. Lopes, L.B. Osorio, and A.T. de Almeida, "Robust Hand Gesture Recognition with a Double Channel Surface EMG Wearable Armband and SVM Classifier," *Biomedical Signal Processing and Control*, vol. 46, pp. 121-130, 2018.
- [12] G.R. Naik, A.H. Al-Timemy, H.T. Nguyen, "Transradial Amputee Gesture Classification using an Optimal Number of sEMG Sensors: an Approach using ICA Clustering," *IEEE Trans. Neural Syst. Rehabil. Eng.*, vol. 24, no. 8, pp. 837-846, 2015.
- [13] S. Pizzolato *et al.*, "Comparison of Six Electromyography Acquisition Setups on Hand Movement Classification Tasks," *PLoS ONE*, vol. 12, no. 10, pp. 1-7, 2017.
- [14] M. Atzori, M. Cognolato, and H. Müller, "Deep Learning with Convolutional Neural Networks Applied to Electromyography Data: A Resource for the Classification of Movements for Prosthetic Hands," *Frontiers in neurorobotics* 10, p.9, 2016.
- [15] A. K. Clarke *et al.*, "Deep Learning for Robust Decomposition of High-Density Surface EMG Signals," *IEEE Trans. Biomed. Eng.*, 2020, In Press.
- [16] E. Rahimian, S. Zabihi, S. F. Atashzar, A. Asif, and A. Mohammadi, "Surface EMG-Based Hand Gesture Recognition via Hybrid and Dilated Deep Neural Network Architectures for Neurorobotic Prostheses," *Journal of Medical Robotics Research*, 2020, pp. 1-12.
- [17] E. Rahimian, S. Zabihi, F. Atashzar, A. Asif, A. Mohammadi, "XceptionTime: Independent Time-Window XceptionTime Architecture for Hand Gesture Classification," *International Conference on Acoustics, Speech, and Signal Processing (ICASSP)*, 2020.
- [18] E. Rahimian, S. Zabihi, S. F. Atashzar, A. Asif, and A. Mohammadi, "Semb-based Hand Gesture Recognition via Dilated Convolutional Neural Networks," *IEEE Global Conference on Signal and Information Processing (GlobalSIP)*, 2019.
- [19] E. Rahimian, S. Zabihi, S. F. Atashzar, A. Asif, and A. Mohammadi, "Semb-based Hand Gesture Recognition via Dilated Convolutional Neural Networks," *IEEE Global Conference on Signal and Information Processing (GlobalSIP)*, 2019.
- [20] W. Wei *et al.*, "A Multi-stream Convolutional Neural Network for sEMG-based Gesture Recognition in Muscle-computer Interface," *Pattern Recognition Letters*, 119, pp. 131-138, 2019.
- [21] W. Wei, Y.Wong, Y. Du, Y. Hu, M. Kankanhalli, W. Geng, "A multi-stream Convolutional Neural Network for sEMG-based Gesture Recognition in Muscle-computer Interface," *Pattern Recognition Letters*, 2017.
- [22] A. Vaswani *et al.*, "Attention is All You Need," *arXiv preprint arXiv:1706.03762*, 2017a.
- [23] J. Devlin, M.W. Chang, K. Lee, and K. Toutanova, "Bert: Pre-training of Deep Bidirectional Transformers for Language Understanding," *arXiv preprint arXiv:1810.04805*, 2018.
- [24] A. Dosovitskiy *et al.*, "An Image is Worth 16x16 Words: Transformers for Image Recognition at Scale," *arXiv preprint arXiv:2010.11929*, 2020.
- [25] G. Krishna, C. Tran, M. Carnahan, and A.H. Tewfik, "EEG based Continuous Speech Recognition using Transformers," *arXiv preprint arXiv:2001.00501*, 2019.
- [26] M. Atzori, *et al.*, "Electromyography Data for Non-Invasive Naturally-Controlled Robotic Hand Prostheses," *Scientific data* 1, no. 1, pp. 1-13, 2014.
- [27] A. Gijsberts, *et al.*, "Movement Error Rate for Evaluation of Machine Learning Methods for sEMG-based Hand Movement Classification," *IEEE Trans. Neural Syst. Rehabil. Eng.*, vol. 22, no. 4, pp. 735-744, 2014.
- [28] M. Atzori *et al.*, "A Benchmark Database for Myoelectric Movement Classification," *IEEE Trans. Neural Syst. Rehabil. Eng.*, 2013.
- [29] U. Côté-Allard, *et al.*, "Interpreting Deep Learning Features for Myoelectric Control: A Comparison with Handcrafted Features," *Frontiers in bioengineering and biotechnology*, 8, p.158, 2020.
- [30] R. N. Khushaba and S. Kodagoda, "Electromyogram (EMG) feature reduction using mutual components analysis for multifunction prosthetic fingers control," *12th Int. Conf. Control Autom. Robot. Vis.(ICARCV)*, 2012, pp. 1534-1539.
- [31] X. Zhai, B. Jelfs, R. H. Chan, and C. Tin, "Self-recalibrating Surface EMG Pattern Recognition for Neuroprosthesis Control based on Convolutional Neural Network," *Frontiers in neuroscience*, 11, p.379, 2017.
- [32] Z. Ding, *et al.*, "sEMG-based Gesture Recognition with Convolution Neural Networks," *Sustainability* 10, no. 6, p. 1865, 2018.
- [33] F. Quivira, *et al.*, "Translating sEMG Signals to Continuous Hand Poses Using Recurrent Neural Networks," in *Proc. IEEE EMBS Int. Conf. Biomed. Health Informat.*, 2018, pp. 166-169.
- [34] T. Sun, Q. Hu, P. Gulati, and S.F. Atashzar, "Temporal Dilation of Deep LSTM for Agile Decoding of sEMG: Application in Prediction of Upper-limb Motor Intention in NeuroRobotics.," *IEEE Robotics and Automation Letters*, 2021.
- [35] S. Bai, J.Z. Kolter, and V. Koltun, "An Empirical Evaluation of Generic Convolutional and Recurrent Networks for Sequence Modeling," *arXiv preprint arXiv:1803.01271*, 2018.
- [36] J. Guan, W. Wang, P. Feng, X. Wang, and W. Wang, "Low-Dimensional Denoising Embedding Transformer for ECG Classification," *International Conference on Acoustics, Speech and Signal Processing (ICASSP)*, 2021, pp. 1285-1289.
- [37] Y. Song, X. Jia, L. Yang, and L. Xie, "Transformer-based Spatial-Temporal Feature Learning for EEG Decoding," *arXiv preprint arXiv:2106.11170*, 2021.
- [38] T.B. Brown, *et al.*, "Language Models are Few-shot Learners," *arXiv preprint arXiv:2005.14165*, 2020.
- [39] Y. Wang, *et al.*, "Transformer-based Acoustic Modeling for Hybrid Speech Recognition," *International Conference on Acoustics, Speech and Signal Processing (ICASSP)*, 2020, pp. 6874-6878.
- [40] B. Hudgins, P. Parker, and R.N. Scott, "A New Strategy for Multifunction Myoelectric Control," *IEEE Trans. Biomed. Eng.*, vol. 40, no. 1, p.82-94, 1993.
- [41] JL Ba, JR Kiros, and G.E. Hinton, "Layer normalization," *arXiv preprint arXiv:1607.06450*, 2016.
- [42] DP. Kingma, and J. Ba, "Adam: A Method for Stochastic Optimization," *ICLR*, 2015.
- [43] U. Côté-Allard, *et al.*, "Deep Learning for Electromyographic Hand Gesture Signal Classification using Transfer Learning," *IEEE Trans. Neural Syst. Rehabil. Eng.*, vol. 27, no. 4, pp. 760-771, 2019.
- [44] F. Wilcoxon, "Individual comparisons by ranking methods," *Biometrics Bull.*, vol. 1, no. 6, pp. 80-83, 1945.